Article

Molecular Cell

Endoplasmic Reticulum Transport of Glutathione by Sec61 Is Regulated by Ero1 and Bip

Graphical Abstract

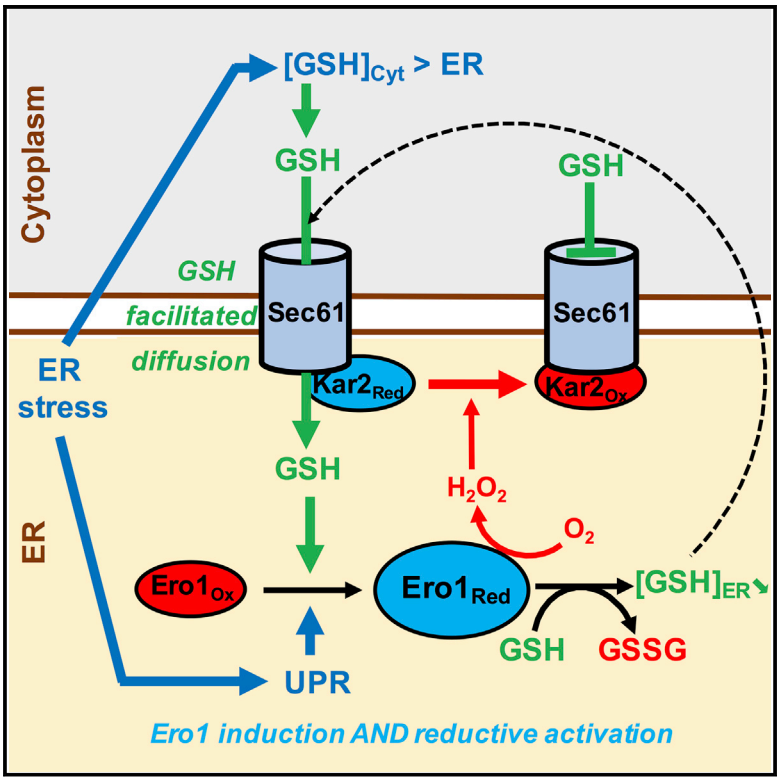

Highlights

- Cytosol-to-ER glutathione transport proceeds via facilitated diffusion through Sec61
- Ero1-dependent Bip (Kar2) oxidation inhibits ER-to-cytosol glutathione transport
- ER-to-cytosol transport of glutathione and Ero1 activation are reciprocally regulated
- Coupling of glutathione transport to Ero1 activation preserves the ER redox poise

Authors

Alise J. Ponsero, Aeid Igbaria, Maxwell A. Darch, ..., Benoit D'Autréaux, Agnès Delaunay-Moisan, Michel B. Toledano

Correspondence

michel.toledano@cea.fr

In Brief

Ponsero et al. show that cytosol-to-ER transport of glutathione proceeds via facilitated diffusion through Sec61. Upon import, glutathione activates Ero1 by reduction, causing Bip oxidation and inhibition of glutathione transport. Coupling of glutathione ER import to Ero1 activation provides a basis for glutathione ER redox poise maintenance.

Ponsero et al., 2017, Molecular Cell 67, 1–12
September 21, 2017
http://dx.doi.org/10.1016/j.molcel.2017.08.012

CellPress

Please cite this article in press as: Ponsero et al., Endoplasmic Reticulum Transport of Glutathione by Sec61 Is Regulated by Ero1 and Bip, Molecular Cell (2017), http://dx.doi.org/10.1016/j.molcel.2017.08.012

Molecular Cell
Article

Endoplasmic Reticulum Transport of Glutathione by Sec61 Is Regulated by Ero1 and Bip

Alise J. Ponsero,[1,5] Aeid Igbaria,[1,4,5] Maxwell A. Darch,[2] Samia Miled,[1] Caryn E. Outten,[2] Jakob R. Winther,[3] Gael Palais,[1] Benoit D'Autréaux,[1] Agnès Delaunay-Moisan,[1] and Michel B. Toledano[1,6,*]
[1]Institute for Integrative Biology of the Cell (I2BC), CEA–Saclay, CNRS, Université Paris–Saclay, ISVJC/SBIGEM, Laboratoire Stress Oxydant et Cancer, 91191 Gif-sur-Yvette, France
[2]Department of Chemistry and Biochemistry, University of South Carolina, Columbia, SC 29208, USA
[3]Department of Biology, University of Copenhagen, 2200 Copenhagen N, Denmark
[4]Present address: Department of Medicine, University of California, San Francisco, San Francisco, CA 94143, USA
[5]These authors contributed equally
[6]Lead Contact
*Correspondence: michel.toledano@cea.fr
http://dx.doi.org/10.1016/j.molcel.2017.08.012

SUMMARY

In the endoplasmic reticulum (ER), Ero1 catalyzes disulfide bond formation and promotes glutathione (GSH) oxidation to GSSG. Since GSSG cannot be reduced in the ER, maintenance of the ER glutathione redox state and levels likely depends on ER glutathione import and GSSG export. We used quantitative GSH and GSSG biosensors to monitor glutathione import into the ER of yeast cells. We found that glutathione enters the ER by facilitated diffusion through the Sec61 protein-conducting channel, while oxidized Bip (Kar2) inhibits transport. Increased ER glutathione import triggers H_2O_2-dependent Bip oxidation through Ero1 reductive activation, which inhibits glutathione import in a negative regulatory loop. During ER stress, transport is activated by UPR-dependent Ero1 induction, and cytosolic glutathione levels increase. Thus, the ER redox poise is tuned by reciprocal control of glutathione import and Ero1 activation. The ER protein-conducting channel is permeable to small molecules, provided the driving force of a concentration gradient.

INTRODUCTION

The small thiol glutathione (GSH) is a ubiquitous nucleophile and cellular thiol-reducing buffer by virtue of its abundance. Together with glutaredoxins, glutathione acts to reduce disulfide bonds, and it is in turn oxidized to glutathione disulfide (GSSG), which is reduced by nicotinamide adenine dinucleotide phosphate reduced (NADPH)-dependent glutathione reductase (Toledano et al., 2007). In *S. cerevisiae*, both glutathione biosynthesis and degradation take place in the cytosol, while glutathione reductase is only present in the cytosol and mitochondrial matrix (Toledano et al., 2007). Thus, GSH/GSSG pools in the other cell compartments are insulated from systems that govern glutathione homeostasis. In these compartments, GSH/GSSG pools adopt very different redox potentials (E_{GSH}) that vary from −289 mV in the cytosol (Østergaard et al., 2004) to −240 mV in the endoplasmic reticulum (ER) (Delic et al., 2010). These subcellular differences presumably reflect differences in glutathione redox functions and suggest the need for regulated fluxes of glutathione and GSSG between the cytosol and these compartments to maintain subcellular glutathione homeostasis.

The ER offers a unique setting with regard to glutathione homeostasis. It contains the thiol oxidase Ero1, which catalyzes the formation of disulfides transmitted to folding substrates via protein disulfide isomerase (Pdi1) (Frand and Kaiser, 1999; Pollard et al., 1998). Ero1 is itself regulated by negative feedback via regulatory disulfides that are thought to form when the ER becomes too oxidized (Sevier et al., 2007). A net ER reducing power is also required by Pdi1 for isomerization of these disulfides into their native arrangement and for reduction of terminally misfolded proteins before retrotranslocation (Margittai and Sitia, 2011). In the ER, glutathione is suspected of providing this reducing power (Chakravarthi and Bulleid, 2004; Cuozzo and Kaiser, 1999; Molteni et al., 2004). Since glutathione is oxidized, but not reduced, in the ER, glutathione must be imported into the ER, while GSSG is exported to the cytosol. Further, as glutathione paradoxically promotes ER oxidation by Ero1 reductive activation (Kumar et al., 2011), the glutathione and GSSG ER-to-cytosol fluxes must be regulated to maintain the ER redox poise.

We have addressed here the mechanism of glutathione trafficking into the ER of *S. cerevisiae*. We found that the ER import of glutathione occurs by facilitated diffusion through the ER Sec61-protein-conducting channel and is regulated by the ER Hsp70 Kar2 (Bip). We also found that glutathione transport is stimulated by ER stress through an increase in the levels of both Ero1, which is set by the unfolded protein response (UPR), and cellular glutathione. Based on these data, we propose a model establishing reciprocal control between the ER import of glutathione and Ero1 activation, which functions to maintain ER redox poise. These data also suggest that the ER protein-conducting channel is generally permeable to small molecules.

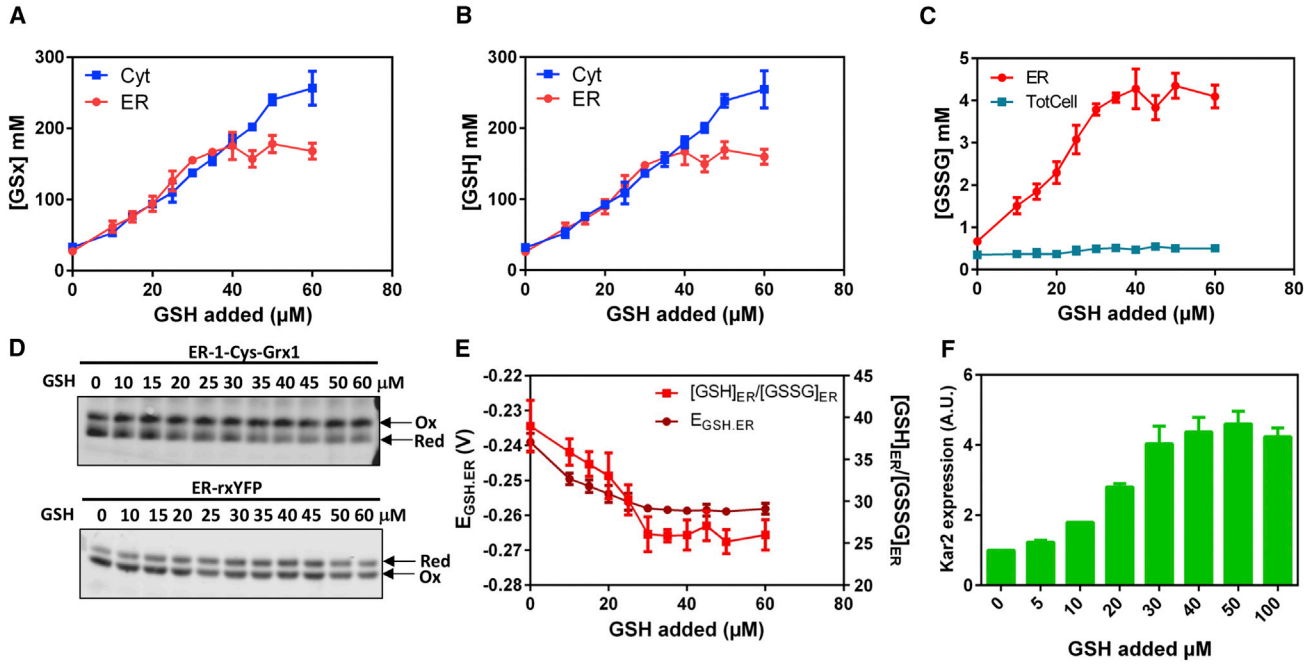

Figure 1. Inhibitable Facilitated Diffusion of Glutathione across the ER Membrane

(A–C) Corrected cytosolic (Cyt) (TotCell × 4.5), total cellular (TotCell), and ER (ER) levels of [GSx] = [glutathione] + 2[GSSG] (A), reduced [glutathione] (B), and oxidized [GSSG] (C) (in millimoles), as indicated, measured in HGT1 cells incubated 1 hr with the indicated amount of glutathione.

(D) Non-reducing SDS-PAGE migration of ER-1-Cys-Grx1 (top) and ER-rxYFP (bottom) from lysates of HGT1 cells incubated with indicated amount of glutathione for 1 hr, representative of those used to derive the data in (E).

(E) The ER glutathione redox potential ($E_{GSH.ER}$) and ER ratio of glutathione/GSSG values used to derive the data in (A)–(C).

(F) *KAR2* expression measured by qPCR in HGT1 cells incubated 1 hr with the indicated amount of glutathione.

Values are the mean of three independent biological replicas ± SD.

RESULTS

The Concentration of Glutathione in the ER and Cytosol Is Equal

To monitor glutathione fluxes across the ER membrane, we accessed its absolute concentration in the cytosol ($[GSx]_{Cyt}$) and ER ($[GSx]_{ER}$) with the use of two distinct glutathione biosensors (Montero et al., 2013). The dithiol yellow fluorescent protein (YFP)-based glutathione biosensor (rxYFP) equilibrates with glutathione in a manner proportional to the $[GSH]^2/[GSSG]$ ratio (Østergaard et al., 2004). The second sensor is 1-Cys-Grx1, a mutant of glutaredoxin 1 (Grx1) with a Cys-to-Ser substitution of its resolving cysteine that equilibrates in a manner proportional to the GSH/GSSG ratio (Iversen et al., 2010). The concentration of GSx ([GSx] = [glutathione] + 2[GSSG]) is calculated from the experimental values obtained with the two probes (Figures 1D and 2D; STAR Methods). Probes were expressed in the cytosol with no targeting signals and in the ER by insertion of the Mns1-signal peptide at the N terminus and ER retrieval HDEL motif at the C terminus (ER-rxYFP, ER-1-Cys-Grx1). Proper ER localization was verified by fluorescence microscopy and cell fractionation (Figure S1). The 1-Cys-Grx1 probe relies on formation of a mixed disulfide between the enzyme and glutathione. However, due to the highly reducing nature of the wild-type (WT) cytosol, this disulfide cannot form, thus preventing measurement of $[GSx]_{Cyt}$. We instead used a strain lacking glutathione reductase (Δ*glr1*) that has a more oxidizing cytosol (Hu et al., 2008), which allowed measuring a $[GSx]_{Cyt}$ value of 31.1 mM (Table 1). Although this concentration is 4.5-fold higher than the GSx value (7.14 ± 1.0 mM) estimated by enzyme assay of whole lysates from the same cells ($[GSx]_{TotCell}$), it is compatible with estimates of the yeast cytosolic distribution volume to account for 20%–30% of the total cell volume. We thus used in this study the 4.5-fold corrected value of $[GSx]_{TotCell}$ as a proxy of $[GSx]_{Cyt}$ ($[GSx]_{Corr.Cyt}$) in WT cells. Note that as measured in Δ*glr1*, $[GSSG]_{Corr.Cyt}$ is higher than $[GSSG]_{Cyt}$ (1.83 ± 0.23 versus 0.50 ± 0.03 mM), as it includes a vacuolar pool of GSSG (Morgan et al., 2013), hence precluding application of the $[GSx]_{TotCell}$ correction to $[GSSG]_{Cyt}$. Table 1 compares the measured glutathione parameters in the ER and cytosol of WT and Δ*glr1*. In the cytosol, E_{GSH} was more oxidizing in Δ*glr1* than in WT (−246 ± 2 mV versus > −289 mV) (Hu et al., 2008) and, as expected, more oxidizing in the ER relative to the cytosol, with the ER of Δ*glr1* slightly more oxidizing than WT (−235 ± 3 mV versus −242 ± 2 mV). Remarkably, $[GSx]_{ER}$ was in the close range of, if not equal to, $[GSx]_{Cyt}$ as measured in both Δ*glr1* (31 ± 1 mM versus 31 ± 1 mM) and WT (30 ± 2 mM versus 29.6 ± 2 mM), in contrast to $[GSSG]_{ER}$, which, as measured in Δ*glr1*, was more than twice its value in the cytosol (1.2 ± 0.03 mM versus 0.5 ± 0.03 mM).

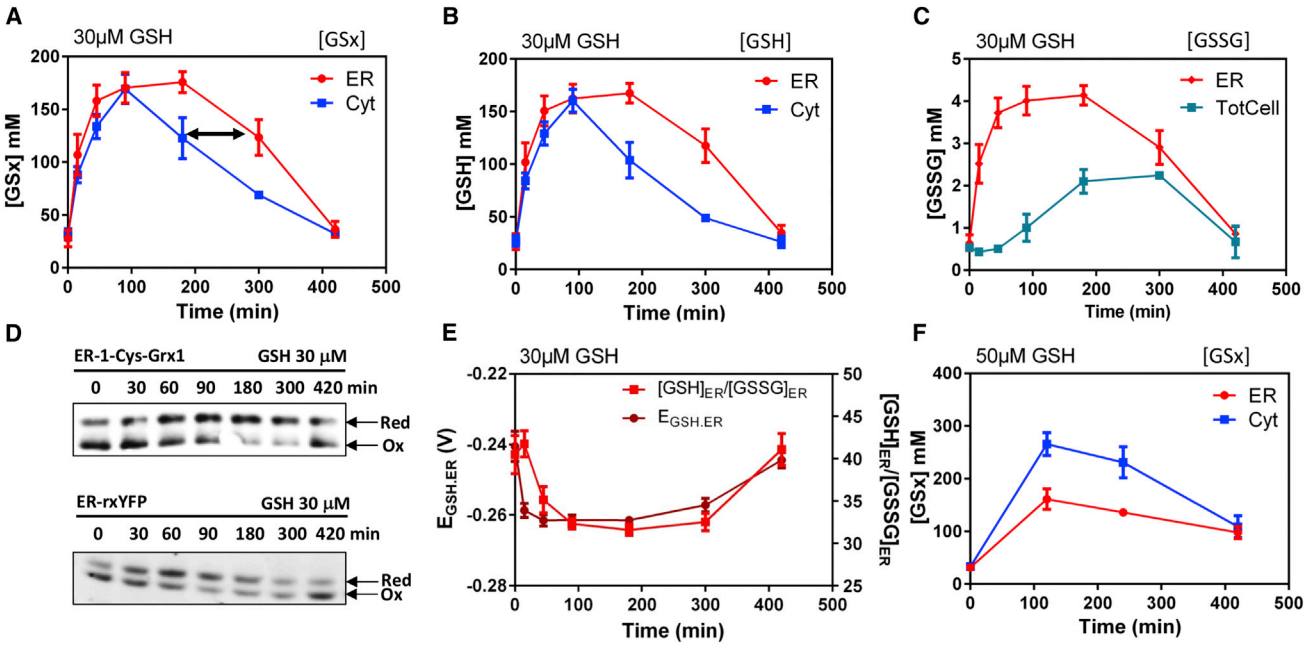

Figure 2. The Time-Dependent Facilitated Diffusion of Glutathione in the ER at High Glutathione Cytosolic Concentrations

(A–C) Corrected cytosolic (Cyt), total cellular (TotCell) and ER (ER) levels, as indicated, of [GSx] = [glutathione] + 2[GSSG] (A), reduced [glutathione] (B), and oxidized [GSSG] (C) measured in HGT1 cells incubated with 30 μM glutathione for the indicated time.

(D) Non-reducing SDS-PAGE migration of ER-1-Cys-Grx1 (top) and ER-rxYFP (bottom) from lysates of HGT1 cells incubated with 30 μM glutathione for the indicated time, representative of those used to derive the data in (E).

(E) The ER glutathione redox potential ($E_{GSH.ER}$) and ER ratio of glutathione/GSSG values used to derive the data in (A)–(C).

(F) Same as in (A), but with 50 μM glutathione.

Values are the mean of three independent biological replicas ± SD.

An Inhibitable Facilitated Diffusion of Glutathione across the ER Membrane

WT cells that overproduce the plasma membrane high-affinity glutathione transporter Hgt1p, hereafter referred to as HGT1 cells, accumulate fairly high levels of glutathione when supplied with glutathione (Kumar et al., 2011). A $[GSx]_{Corr.Cyt}$ plateau of 250 mM is reached 1 hr after addition of 60 μM glutathione to the medium (Figures 1A and S2A). We used HGT1 cells as a tool to monitor cytosol-to-ER fluxes of glutathione, since this flux is amplified at high cellular glutathione levels. To validate the $[GSx]_{TotCell}$ correction in these cells, we compared the HGT1-Δ*glr1* values of $[GSx]_{TotCell}$ and $[GSx]_{Cyt}$ 1 hr after addition of increasing amounts of glutathione. These values were aligned throughout the glutathione titration, provided the 4.5-fold correction was applied to $[GSx]_{TotCell}$ (Figure S2B). Incubating HGT1 cells 1 hr with increasing amounts of glutathione led to an increase in $[GSx]_{ER}$ that tightly paralleled the $[GSx]_{Corr.Cyt}$ increase, up to a plateau lower than the $[GSx]_{Corr.Cyt}$ plateau (170 versus 250 mM) reached at 30 μM glutathione (Figure 1A). Reduced glutathione constituted most of the GSx that had entered the ER, thereby decreasing $E_{GSH.ER}$ (Figures 1B and 1E). As glutaredoxins catalyze rxYFP equilibration with the glutathione redox couple, we verified $E_{GSH.ER}$ using an ER-rxYFP-Grx1 fusion, which gave almost identical values (Figure S2C). We also verified proper ER localization of the probes in HGT1 cells loaded with glutathione by fluorescence microscopy, use of the rxYFP variant carrying a glycosylation site, and cell fractionation (Figures S2D–S2F). Thus, $[GSx]_{Corr.Cyt}$ and $[GSx]_{ER}$ steady-state values are in the same range (Table 1), and any increase in $[GSx]_{Corr.Cyt}$ causes a similar increase in $[GSx]_{ER}$, which suggests that glutathione is imported into the ER along its concentration gradient across the ER membrane. Importantly, the lower [GSx] plateau reached in the ER, relative to the cytosol, indicates that transport is inhibited when $[GSx]_{Corr.Cyt}$ ~170 mM. ER ingress of glutathione activates Ero1 by reduction (Figure S6) (Kumar et al., 2011). This was manifested here by a $[GSSG]_{ER}$ increase from 0.6 mM to a 4-mM plateau coincident with the $[GSx]_{ER}$ plateau, which slightly decreased $[GSH]_{ER}/[GSSG]_{ER}$ (Figures 1C, 1D, S2G, and S2H). Increased ER glutathione levels caused ER stress, as shown by UPR-dependent *KAR2* induction (Kumar et al., 2011). The induction amplitude was also proportional to the amount of glutathione added, up to a plateau reached at the levels of added glutathione that inhibit glutathione ER import (Figure 1F).

The time course of the HGT1 cells response to 30 μM glutathione showed that $[GSx]_{Corr.Cyt}$ peaked at 170 mM, 1.5 hr after glutathione addition, and slowly declined to the pretreatment level at 7 hr (Figure 2A). Here again, $[GSx]_{ER}$ tightly paralleled the $[GSx]_{Corr.Cyt}$ increase, but interestingly, its decline was delayed, and $[GSx]_{ER}$ was significantly higher than $[GSx]_{Corr.Cyt}$ at the 3- and 5-hr time points (Figure 2A, black arrow). This result suggests that the concentration-dependent transport that drives

Table 1. Glutathione Parameters Measured in Exponentially Growing Wild-Type and Δ*glr1* Cells

	[GSx] (mM)[a]	[GSH] (mM)	[GSSG] (mM)	E_{GSH} (mV)	[GSH]/[GSSG]
WT					
ER[b]	30 ± 2	29.6 ± 2	0.60 ± 0.04	−242 ± 2	42 ± 2
TotCell[c]	7 ± 1	6.6 ± 1	0.40 ± 0.05	−289[d]	N/A
Cor TotCell[e]	31. 5 ± 4.5	29.7 ± 4.5	N/A[f]	−289[d]	N/A
Δglr1					
ER[b]	31 ± 1	29 ± 1	1.20 ± 0.03	−235 ± 3	22 ± 2
Cytosol[g]	31 ± 1	30 ± 1	0.50 ± 0.03	−246 ± 2	46 ± 3
TotCell[c]	7.14 ± 1	6.44 ± 1	0.40 ± 0.05	N/A	N/A
Cor TotCell[e]	32.13 ± 4.5	28.98 ± 4.5	1.80 ± 0.23	N/A	N/A

Cor, corrected; N/A, not applicable.
[a][GSx] = [GSH] + 2[GSSG].
[b]Calculated from data obtained using ER-rxYFP and ER-1-Cys-Grx1.
[c]Measured in total cell lysates by enzyme assay.
[d]Established in Østergaard et al. (2004).
[e]4.5-fold corrected value of $[GSx]_{TotCell}$ (see Results; Figure S2).
[f]The correction cannot be applied to GSSG, as TotCell also contains the vacuolar GSSG.
[g]Calculated from data obtained using Cyt-rxYFP and Cyt-1-Cys-Grx1.

glutathione ER ingress does not operate in reverse under this condition. Here again, reduced glutathione constituted most of the GSx that entered the ER, along with Ero1-dependent $[GSSG]_{ER}$ increase, which interestingly was followed by an increase in $[GSSG]_{TotCell}$ (Figures 2B and 2C). As the latter originates from Ero1 activity (Figures S2G and S2H), glutathione must exit the ER, at least in part, upon conversion into GSSG. These perturbations in glutathione and GSSG levels led to a transient decrease in both E_{GSH} and the glutathione/GSSG ratio in the ER (Figures 2D and 2E). At 50 μM added glutathione, $[GSx]_{Corr.Cyt}$ reached much higher values relative to $[GSx]_{ER}$ (Figure 2F), indicating again glutathione transport inhibition (see Figure 1A).

We conclude that glutathione is transported from the cytosol to the ER along a concentration gradient, which suggests a facilitated diffusion and hence the presence of a glutathione transporter. Further, transport is inhibited when $[glutathione]_{Cyt}$ reaches ~170 mM. Once the ER is saturated with glutathione, glutathione re-export to the cytosol appears inhibited.

A Screen for an ER Glutathione Transporter Identifies Sec61

Glutathione becomes toxic at the high levels that it reaches in HGT1 cells, inhibiting growth and causing cell death (Figures S3A and S3B). This occurs mainly, if not exclusively, by impacting the ER, since HGT1 cells lacking the UPR regulator Ire1p are sensitive to glutathione at concentrations that are nontoxic to HGT1 cells (Kumar et al., 2011). Based on this notion, we assumed that impairment of the ER import of glutathione should mitigate glutathione toxicity, providing a means of screening for candidate glutathione transporters. We screened null and temperature-sensitive (ts) mutations of genes encoding ER transmembrane proteins that would both confer tolerance to HGT1-dependent glutathione toxicity without impairing glutathione accumulation. We thereby identified the *sec61-2* ts allele of the essential gene *SEC61*, which encodes the universally conserved ER protein-conducting channel (Deshaies and Schekman, 1987). In HGT1-*sec61-2* cells, glutathione accumulation upon glutathione addition was similar at the non-restrictive (24°C) and restrictive (37°C) temperatures, which indicated the correct plasma membrane expression of Hgt1p (Figure 3A). In striking contrast, HGT1-*sec61-2* cells remained viable at 37°C, whereas they lost viability at 24°C, similar to HGT1 cells at both 24°C and 37°C (Figure 3B). We sought to evaluate whether the increased resistance to glutathione toxicity was due to defective ER import of glutathione by monitoring glutathione cytosol-to-ER traffic via measurement of $E_{GSH.ER}$. However, ER-rxYFP was highly reduced at steady state in *sec61-2* cells due to probe mislocalization in the cytosol (Figure S3C), thereby precluding this experiment.

In yeast, protein translocation into the ER occurs either through a cotranslational, signal-recognition particle (SRP)-dependent pathway that uses the heterotrimeric Sec61 complex made of Sec61, Sbh1, and Sss1 or through a post-translational translocation pathway that uses the heptameric Sec complex made of the Sec61 complex plus the Sec62-Sec63 complex (Mandon et al., 2013). SRP-dependent translocation also uses a Sec61-alternate translocon made of the Sec61-distantly related pore Ssh1, which complexes with Sbh2 and Sss1. Based on the above data, we reexamined the *sec62-1* (Deshaies and Schekman, 1990) and *sec63-1* (Rothblatt et al., 1989) ts mutants of the essential genes *SEC62* and *SEC63*. However, both mutants retained full HGT1-dependent glutathione sensitivity at both 24°C and 37°C (Figures 3C, 3D, S3E, and S3F).

These data suggest that the SRP-dependent pathway, but not the post-translational protein translocation pathway, is involved in the ER import of glutathione. We next sought further proof of the role of Sec61 in this transport.

Both Sec61 and Ssh1 Transport Glutathione into the ER

The ten transmembrane (TM) spans of Sec61 are arranged into two halves that form an hourglass-shaped pore with a middle ring and a lateral gate between transmembrane domain 2 (TM2) and TM7 facing the lipid phase. Its lumenal face is filled by the plug domain, a reentry loop preceding TM2 (Park and Rapoport, 2012). In the Sec61 closed conformation, the lateral gate is closed, and both the ring and plug domain maintain the channel permeability seal. In yeast, a gating motif that links the Sec61 lateral gate and plug domain regulates the transition from the closed to open channel conformation (Trueman et al., 2012). The *sec61ΔL7* mutant lacks the entire lumenal loop 7 adjacent to the lateral gate motif, which impairs transition from the closed to the open conformation, thereby causing defective post-translational translocation, slow growth, and cold sensitivity (Tretter et al., 2013). When transformed with HGT1, the *sec61ΔL7* mutant accumulated glutathione as WT, which indicated correct Hgt1p plasma membrane expression, but was highly resistant to glutathione-induced cell death (Figures 4A, 4B, and S4B). Furthermore, in HGT1-*sec61ΔL7*, the decrease of $E_{GSH.ER}$

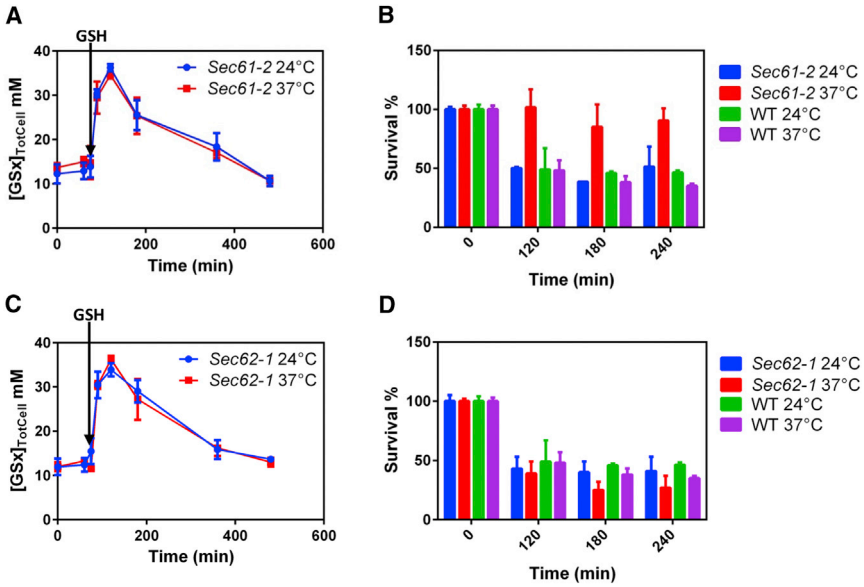

Figure 3. A Screen Identifies the ER Sec61 Protein-Conducting Channel as the ER Glutathione transporter

(A and C) Total cellular levels (TotCell) of [GSx] in whole-cell lysates of HGT1-*sec61-2* (A) or HGT1-*sec62-1* (C) cells. Cells were grown at 24°C and then switched to 37°C or left at 24°C, as indicated, 45 min prior to glutathione addition (30 μM) (arrow) and then incubated for the indicated time.

(B and D) Glutathione survival assay. HGT1-*sec61-2* (B) or HGT1-*sec62-1* (D) cells were grown to the exponential phase at 24°C, switched to 37°C or left at 24°C, as indicated, 1 hr prior to adding glutathione (30 μM), and then incubated for the indicated time. The survival rate is the percentage of colony-forming units per total number of cells at each time point. All values are the mean of three independent biological replicas ± SD.

observed in HGT1 cells on addition of 30 μM glutathione was severely blunted, if not absent (Figure 4C), thus indicating defective ER import of glutathione, in agreement with the viability assay. The N302 residue in TM7 is part of the Sec61 gating motif (Trueman et al., 2012); its substitution to a hydrophobic (N302L) or polar residue (N302D) stabilizes Sec61 in the closed or open conformation, respectively. Consistent with the previous result, in the *sec61*^{N302L} mutant, the decrease of $E_{GSH.ER}$ on addition of 30 μM glutathione was also dampened, thus confirming that mutations stabilizing the Sec61 closed conformation prevent the ER import of glutathione (Figure 4D). Strikingly, expression of *sec61*^{N302L} in a strain lacking *SSH1* (Δ*ssh1*) further impaired transport (Figure 4D), thus suggesting a redundancy of Sec61 and Ssh1 in glutathione transport. In contrast, the Sec61^{N302D} mutation, which stabilizes the open conformation, did not alter the ER import of glutathione (Figure 4E). HGT1-dependent cellular glutathione accumulation (Figure S4C) and proper ER localization of ER-rxYFP (Figures S3C and S3D) was verified for these and the other *sec61* mutants and conditions tested here. In yeast, entire removal of the Sec61 plug domain (Δplug) causes a *prl* phenotype (i.e., the suppression of signal sequence mutations) but no growth defects at any temperature (Junne et al., 2006). In contrast to the above Sec61 mutations, the ER transport of glutathione in the Δplug mutant was similar to WT on addition of 30 μM glutathione (Figure 4F) but differed from the latter at 50 μM (Figure 4G). At this higher level of glutathione, ER reduction was further increased, indicating loss of transport inhibition.

To further establish the role of Sec61 in glutathione transport, we sought to identify conditions under which it becomes operative. Puromycin (Pm), which causes premature chain termination, empties ER translocon pores by release of the nascent chain into the ER lumen without ribosome-pore detachment (Simon and Blobel, 1991). We overproduced Hgt1p in a strain made Pm sensitive by inactivation of the pleiotropic-drug resistance transcription factors Pdr1 and Pdr3 and the methyltransferase Erg6 (Δ*erg6*Δ*pdr1*Δ*pdr3*) (Cary et al., 2014). In this strain, a 15-min treatment with 2 mM Pm did not prevent, but at best slightly increased, reduction of the ER with addition of 50 μM glutathione relative to Pm-untreated cells (Figure 4H), which indicates that the ER import of glutathione does not require de novo protein synthesis. Cycloheximide (CHX) traps the nascent chain within the channel by blocking the translocation step in translation elongation, thereby stabilizing ribosomes on the ER membrane (Schneider-Poetsch et al., 2010). Strikingly, a 10-min treatment with CHX totally prevented reduction of the ER (Figure 4I), despite normal cellular glutathione accumulation (Figure S4E). Hence, actively translating ribosomes bound to translocons effectively prevent glutathione transport. The almost total inhibitory effect of CHX may also indicate that it increases the density of active ER membrane ribosome-bound pores by decreasing their turnover. We next tested whether idle ribosome binding to translocons is required for glutathione transport. Sec61 mutations impairing ribosome binding did not allow proper co-expression of HGT1 and ER-rxYFP. We instead used a plasmid-borne galactose-inducible dominant allele of *SRP54* (*SRP54*^{dn}) defective in GTP hydrolysis, which locks and inactivates the SRP receptor (Mutka and Walter, 2001). We found that 3 hr after Gal1-SRP54^{dn} induction in HGT1 cells, reduction of the ER upon glutathione incubation was decreased relative to cells carrying Gal-SRP54 (Figure 4J), despite normal HGT1-dependent glutathione accumulation (Figure S4D). Longer inhibition of the SRP pathway was not tested since this impaired HGT1 and ER-rxYFP expression. By sequestering the SRP receptor into an inactive pool (Mutka and Walter, 2001), SRP54^{dn} should decrease the ER content of both active and inactive ribosome-bound translocons. However, since the effect of CHX excludes the former, the effect of SRP54^{dn}, even partial, is suggestive of a requirement for inactive ribosome-bound translocons.

Collectively, these data indicate that the Sec61 and Ssh1 translocons serve to transport glutathione across the ER membrane and suggest that this transport requires the presence of inactive ribosomes bound to translocons. Furthermore, whereas

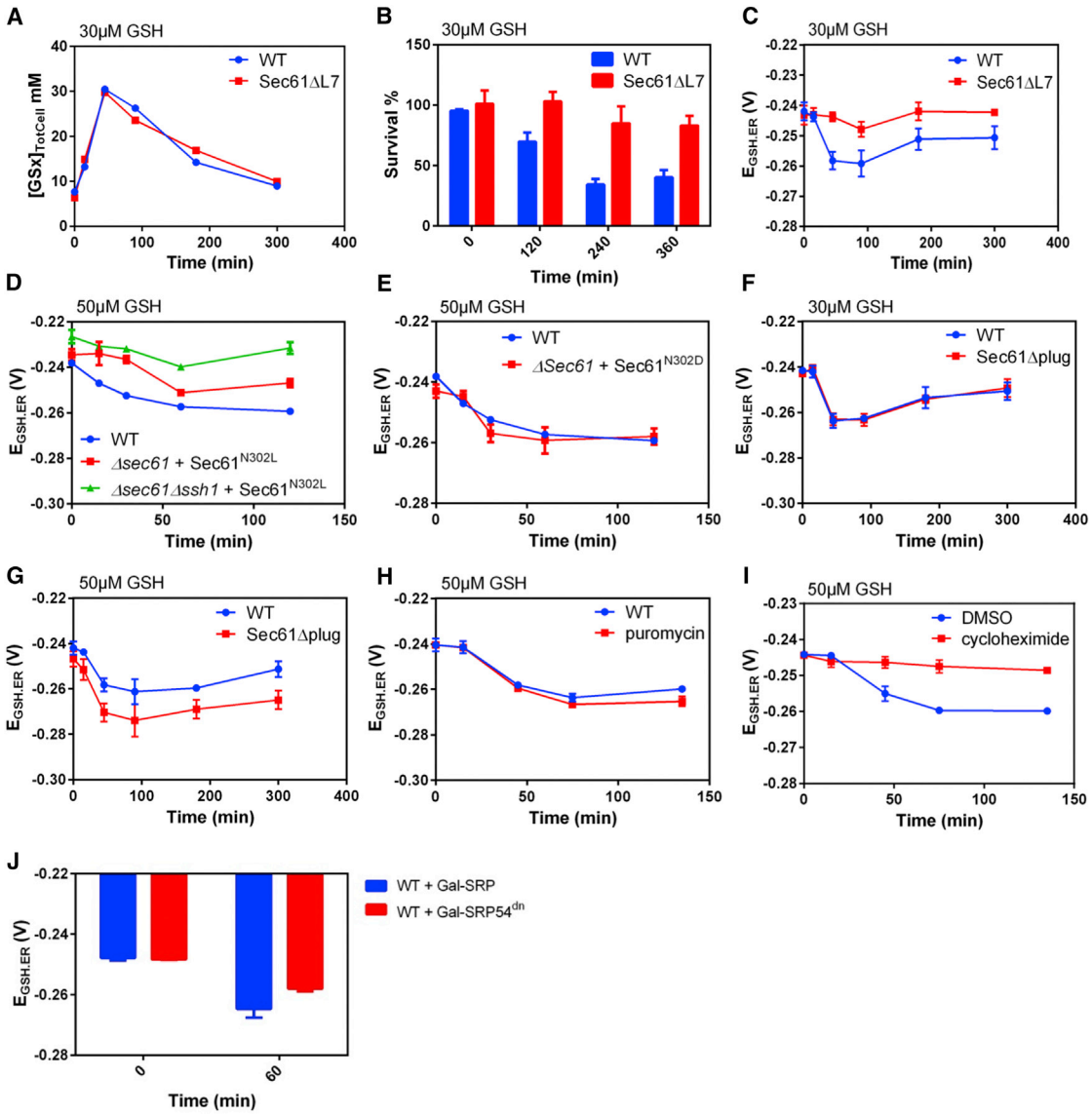

Figure 4. Sec61 and Ssh1 Serve in the ER Transport of Glutathione

(A–C) Total cellular levels (TotCell) (A), survival rate (as in Figures 3B and 3D) (B), and $E_{GSH.ER}$ values (C) in HGT1 and HGT1-Δ*sec61-sec61Δ7* cells incubated with 30 μM glutathione for the indicated times.

(D–G) $E_{GSH.ER}$ values in HGT1 cells (D–G), HGT1-Δ*sec61sec61N302L*, or HGT1-Δ*sec61*Δ*ssh1sec61N302L* as indicated (D), HGT1-Δ*sec61sec61N302D* (E), HGT1-Δ*sec61*Δplug (F and G), incubated during the indicated time with the indicated amount of glutathione.

(H) Value of $E_{GSH.ER}$ in HGT1-Δ*erg6*Δ*pdr1*Δ*pdr3* cells after incubation with 50 μM glutathione during the indicated time. Puromycin (2 mM) was added 20 min prior to glutathione addition.

(I) Value of $E_{GSH.ER}$ in HGT1 cells after incubation with 50 μM glutathione during the indicated time. Cycloheximide (CHX) (200 μg/mL) or vehicle (DMSO) was added 15 min prior to adding glutathione.

(J) Value of $E_{GSH.ER}$ in HGT1 cells expressing *SRP54* or *SRP54*^{dn} from a *GAL1* promoter incubated 60 min with 30 μM glutathione, 3 hr after switching the medium from raffinose to galactose. All values are the mean of three independent biological replicas ± SD.

the Sec61 closed conformation prevents glutathione transport, the plug domain contributes to the mechanism of transport inhibition.

Oxidized Kar2 Inhibits the ER Import of Glutathione

The ER chaperone Kar2 (Bip) is oxidized to a sulfenic acid at residue Cys63 in cells overexpressing Ero1$^{C150\text{-}C295}$, a mutant that is constitutively active due to the lack of negative regulatory disulfides (see introduction). In turn, Kar2 mutants mimicking its oxidized form mitigate Ero1$^{C150\text{-}C295}$ toxicity (Wang et al., 2014). Given Sec61's role in glutathione transport, Kar2's contribution to Sec61 protein translocation (Mandon et al., 2013), and glutathione activation of Ero1 (Figure S6) (Kumar et al., 2011), we examined the involvement of Kar2 in glutathione transport.

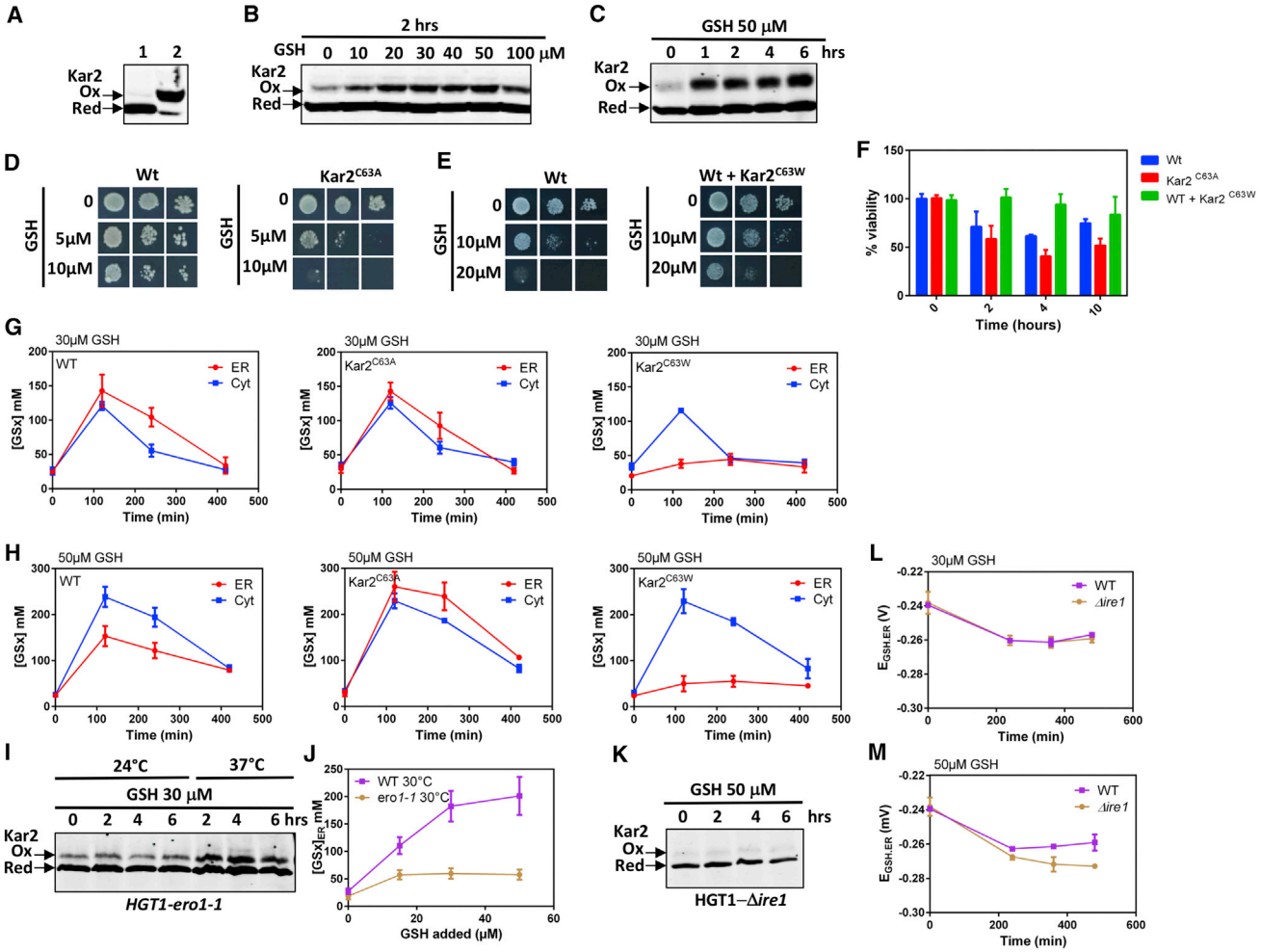

Figure 5. Kar2 Oxidation Inhibits the ER Transport of Glutathione

(A–C) Kar2 redox westerns after SDS-PAGE migration. DTT-reduced samples alkylated by either NEM (lane 1) or PEG-maleimide (lane 2) served as control for reduced and oxidized Kar2 migration, respectively (A). Lysates of HGT1 cells incubated 2 hr with the indicated amount of glutathione, were alkylated with NEM, then reduced and alkylated with Mal-PEG-maleimide (B). Lysates of HGT1 cells incubated with 50 µM glutathione during the time indicated and processed as in (B). The 2-, 4-, and 6-hr samples contain half the amount of lysate relative to untreated (0 hr) samples (C). Data are representative of at least two experiments.

(D and E) Tolerance to glutathione by growth on plates containing the indicated amount of glutathione. HGT1 cells (WT) and HGT1-Δ*kar2* cells expressing Kar2^{C63A} (D); HGT1 cells (WT) expressing or not Kar2^{C63W} (E). Data are representative of at least two experiments.

(F) Survival rates to 50 µM glutathione of the cells used in (D) and (E), as indicated, assayed as in Figures 3B and 3D.

(G and H) Corrected cytosolic (Cyt) (TotCell × 4.5) and ER (ER) levels of [GSx] after incubation with 30 µM (G) or 50 µM glutathione (H) of the cells used in (D) and (E) and during the time indicated.

(I) HGT1-*ero1-1* cells incubated with 30 µM glutathione at the temperature and time indicated were processed as in (B) and (C) for Kar2 oxidation.

(J) ER $[GSx]_{ER}$ levels in HGT1 or HGT1-*ero1-1* cells, as indicated, incubated 2 hr at 30°C with the indicated amount of glutathione.

(K) HGT1-Δ*ire1* cells incubated with 50 µM glutathione for the indicated time and processed for Kar2 oxidation as in (B) and (C).

(L and M) Values of $E_{GSH,ER}$ in HGT1 or HGT1-Δ*ire1* cells incubated with 30 (L) or 50 (M) µM glutathione for the indicated time.

Values in (F)–(H), (J), (L), and (M) are the mean of three independent biological replicas ± SD.

We probed Kar2 oxidation by differential labeling of reduced versus oxidized Cys residues with N-ethylmaleimide (NEM) and polyethylene glycol (PEG)-maleimide, respectively, which upshifts oxidized Kar2 SDS-PAGE migration (Figures 5A, S5A, and S5B). A 2-hr incubation with glutathione triggered Kar2 oxidation, the degree of which was proportional to the amount of added glutathione, up to a maximum at 20–30 µM (Figure 5B). A time-course response to 50 µM glutathione showed that oxidation was maximal between 1 and 4 hr and remained so longer than 6 hr (Figures 5C and S6). To test whether Kar2 oxidation alters glutathione toxicity, we used mutants with substitution of Cys63 to either Ala (Kar2^{C63A}) or Trp (Kar2^{C63W}), which mimics the reduced and sulfenylated forms of Kar2, respectively (Wang et al., 2014). *kar2-C63A* is fully viable, whereas *KAR2-C63W* is unviable and must be complemented by *KAR2* (Wang et al., 2014). We found that relative to HGT1 cells, HGT1-*kar2-C63A*

was more sensitive to glutathione by both growth plate and survival assays, whereas HGT1-*kar2-C63W* was much more resistant (Figures 5D–5F), despite normal HGT1-dependent glutathione accumulation (Figure S4F). Consistent with the sensitivity assays, the ER import of glutathione in HGT1-*kar2-C63A* was not only fully maintained, but as seen with the Δplug mutant, not anymore inhibited, with $[GSx]_{ER}$ equilibrating with $[GSx]_{Corr.Cyt}$ at the very high peak value of 250 mM, 2 hr after addition of 50 μM glutathione (Figures 5G and 5H). In contrast, ER import of glutathione was severely blunted in HGT1 cells expressing *Kar2-C63W*, with $[GSx]_{ER}$ never rising above 45 mM relative to the high $[GSx]_{Corr.Cyt}$ values of 120 and 230 mM seen at 30 and 50 μM added glutathione, respectively (Figures 5G and 5H).

Kar2 is presumably oxidized by the H_2O_2 side product of Ero1 catalysis (Tu and Weissman, 2002). We thus sought to probe the causal links between Kar2 oxidation, Ero1 reductive activation, and glutathione transport inhibition using the *ero1-1* ts mutant (Frand and Kaiser, 1999) to blunt the ER source of H_2O_2. Unexpectedly, however, Kar2 was oxidized in HGT1-*ero1-1* cells at the non-restrictive temperature (24°C) prior to glutathione addition (Figure 5I). Oxidation increased at 37°C, possibly by reactive oxygen species (ROS) originating from mitochondria, but not after glutathione addition (Figure 5I). We took advantage of Kar2 constitutive oxidation in *ero1-1* to directly probe the effect of this modification on glutathione transport. At 37°C, the ER was too reducing to allow any measurements in the HGT1-*ero1-1* strain due to lack of Ero1 activity. However, we found that at 30°C, glutathione transport was substantially inhibited (Figure 5J), confirming the link between Kar2 oxidation and glutathione transport inhibition. We also found that Kar2 was not oxidized in Δ*ire1* with glutathione addition (Figure 5K) as a result of Ero1 defective UPR induction (see below), which increased the threshold glutathione transport inhibition relative to WT (Figures 5L, 5M, S4G, and S4H).

These data indicate that oxidation of Kar2 provides the molecular basis for the inhibitable nature of glutathione transport into the ER, also corroborating the role of Sec61 in this transport.

A Tight Coupling between UPR-Dependent Ero1 Induction and ER Import of Glutathione

As suggested above, by triggering Ero1-dependent Kar2 oxidation, glutathione regulates its own import into the ER. To further establish the coupling between ER glutathione import, Ero1 activity, and Kar2 oxidation, we monitored the glutathione dependence of Kar2 oxidation by Ero1 using the Δ*gsh1* strain that cannot synthesize glutathione. In WT cells, $Ero1^{C150AC295A}$ (Wang et al., 2014) or Ero1 overproduction from a galactose-inducible promoter triggered Kar2 oxidation (Figure 6A). In Δ*gsh1*, however, although Kar2 became oxidized, oxidation was now transient (Figure 6A), disappearing with the degree of glutathione depletion (Figure 6B), thus confirming the links between ER import of glutathione, Ero1 activation, and Kar2 oxidation. We reciprocally tested the influence of $Ero1^{C150AC295A}$ overproduction on the ER import of glutathione, in which facilitated diffusion of glutathione is expected to be stimulated by Ero1-dependent conversion of glutathione into GSSG. When $Ero1^{C150AC295A}$ was induced, $[GSx]_{ER}$ indeed steadily increased up to 80 mM at 8 hr, but unexpectedly $[GSx]_{Corr.Cyt}$ also increased to a similar value (Figures 6C and 6D). Simultaneous increase in both Ero1 activity and $[GSx]_{Corr.Cyt}$ masked which of the two triggers ER import of glutathione. Since perturbation is initiated in the ER, the latter should be a consequence of the former, at least initially, and hence coupling between glutathione import and Ero1 activity is reciprocal. Overproducing WT Ero1 similarly increased both $[GSx]_{ER}$ and $[GSx]_{Corr.Cyt}$, albeit to lower levels (Figures 6C and 6D).

To determine whether the defective Kar2 oxidation in Δ*ire1* (see Figure 5K) is due to faulty Ero1 induction by a disabled UPR, we overproduced Ero1 or its hyperactive mutant in Δ*ire1*. This indeed restored Kar2 oxidation (Figure 6A, bottom), thus indicating that UPR-induced de novo Ero1 synthesis is critical in the coupling between Ero1 and glutathione transport.

We lastly explored the Ero1-glutathione interplay, this time under ER stress caused by tunicamycin (Tm). In WT, addition of 1 μg Tm led to an increase of $[GSx]_{ER}$ from 30 up to 60 mM at 2 hr, which, as in cells overexpressing Ero1, was accompanied by a similar increase of $[GSx]_{Corr.Cyt}$ (Figure 6H). Tm at 0.25 and 0.1 μg also triggered $[GSx]_{ER}$ and $[GSx]_{Corr.Cyt}$ increases of amplitude proportional to the amount of Tm (Figures 6F and 6G). In keeping with the ER import of glutathione, Tm also led to Ero1 activation, as indicated by Kar2 oxidation, with the higher dose of the stressor generating a faster oxidation response (Figure 6I).

In conclusion, our data establish a reciprocal interplay between ER import of glutathione and activation of Ero1, which appears integral to the UPR during ER stress (Figure 6J).

DISCUSSION

As we showed here, glutathione is transported into the ER in *S. cerevisiae* by facilitated diffusion through the universally conserved ER protein-conducting channel Sec61, with oxidized Kar2 inhibiting this transport. Upon import into the ER, glutathione in turn inhibits its import by triggering H_2O_2-dependent Kar2 (Bip) oxidation through Ero1 reductive activation, which indicates reciprocal control between ER glutathione import and Ero1 activation (Figure 6J). We also demonstrated that ER stress stimulates the regulated transport of glutathione by increasing the levels of both cellular glutathione and Ero1. Such reciprocal control of the opposing ER thiol-oxidizing and reducing pathways appears essential for subtle homeostatic control of ER redox poise. This control prevents excessive Ero1 activity, which underlies the toxicity of both overproduction of hyperactive Ero1 (Wang et al., 2014) and high cellular glutathione levels (Kumar et al., 2011). This reciprocal regulation might also be important to satisfy the requirements for oxidative protein folding during ER stress by simultaneously promoting a transient increase in Ero1-dependent thiol oxidation and extra glutathione reducing power. These data also suggest that the ER membrane is permeable to other small molecules in addition to glutathione.

Reciprocal Control of Ero1 Activity and ER Import of Glutathione

The ER transport mechanism of glutathione into the ER includes four critical features. (1) The facilitated diffusion of reduced glutathione that follows the concentration gradient across the ER

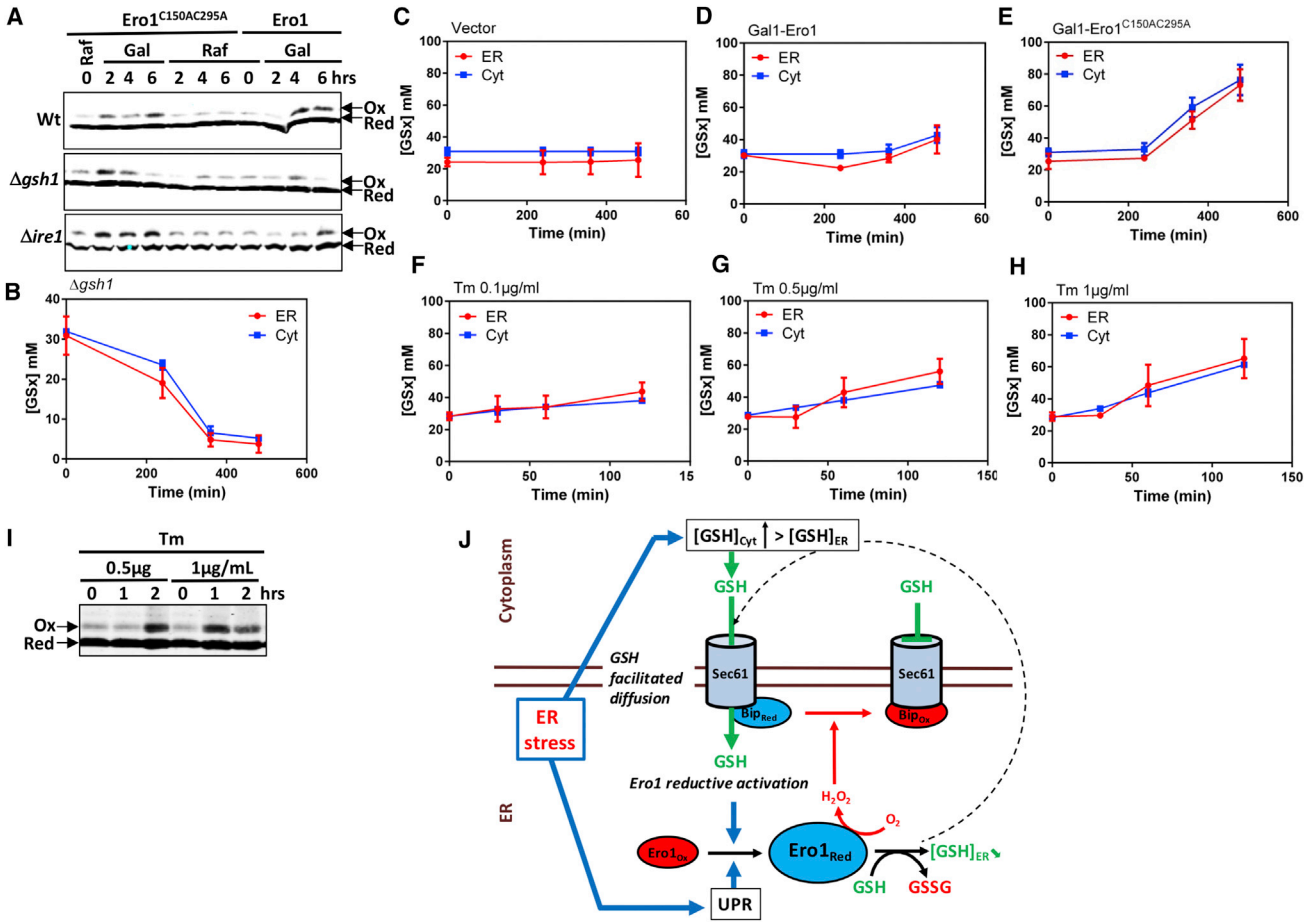

Figure 6. Reciprocal Interplay between the ER Import of Glutathione and Ero1 Activation

(A) Kar2 oxidation in WT, Δ*gsh1*, and Δ*ire1* expressing Ero1^{C150AC295A} or Ero1 from a *GAL1* promoter, as indicated, grown in raffinose or galactose medium for the indicated time and processed as in Figures 5B and 5C.

(B–H) Corrected cytosolic (Cyt) (TotCell × 4.5) and ER (ER) [GSx] in Δ*gsh1* incubated during the indicated time in medium lacking glutathione (B); in HGT1 cells carrying an empty vector (C), Gal1-*ERO1* (D), or Gal1-*ERO1*^{C150AC295A} (E), switched from raffinose to galactose medium at time 0 (C–E); and in WT cells incubated with 0.1 (F), 0.5 (G), or 1 μg/mL (H) tunicamycin (Tm) for the indicated time (F–H).

(I) WT cells incubated with 0.5 or 1 μg/mL tunicamycin (Tm) for the indicated time were processed for Kar2 oxidation as in Figures 5B and 5C. The 1- and 2-hr 0.5 μg/mL Tm samples contain one-half and one-quarter the lysates amount relative to untreated (0 hr), respectively, and the 1- and 2-hr 1 μg/mL samples one-quarter and one-sixth relative to 0 hr. Values in (B)–(H) are the mean of three independent biological replicas ± SD.

(J) Proposed model. ER stress stimulates both [glutathione]$_{Cyt}$ increase and UPR-dependent Ero1 de novo synthesis. [glutathione]$_{Cyt}$ increase stimulates ER facilitated diffusion of glutathione, which promotes Ero1 reductive activation, and further stimulates glutathione import by glutathione oxidation to GSSG. UPR-dependent Ero1 level increase is critical for allowing active Ero1-dependent H_2O_2 production to reach the threshold levels required to oxidize Kar2, which inhibits glutathione import, in turn allowing Ero1 activity to cease.

membrane is essential for maintaining ER glutathione homeostasis, as it compensates for the glutathione consumed in the ER by Ero1-dependent oxidation. Such facilitated glutathione diffusion has been suggested in mammals based on an in vitro microsome transport assay (Bánhegyi et al., 1999). (2) The transport of glutathione is inhibited by the oxidized form of Kar2. These two features establish a reciprocal regulation between glutathione import and activation of Ero1, since Kar2 oxidation is a function of Ero1 activity and Ero1 is activated by (indirect) reduction by glutathione (Figure 6J). The two other features are seen during ER stress, which activate the transport mechanism. (3) The unexpected increase in cytosolic glutathione levels during ER stress, the levels of which are commensurate to stress intensity (Figures 6C–6H), yields a net import of reducing equivalents in the ER. (4) The level of Ero1 set by the UPR in turn sets both the rate of glutathione consumption and the levels of H_2O_2 produced. The critical role of the latter in the regulation of glutathione transport is reflected by lack of Kar2 oxidation and hence of glutathione transport inhibition in cells with a disabled UPR (Figures 5K–5M). Hence, ER stress stimulates glutathione transport in a manner proportional to its intensity by setting the magnitude of both [glutathione]$_{Cyt}$ increase and UPR-dependent Ero1 induction. This effect is reflected by the observation that the concerted increase in [GSH]$_{Cyt}$ and [GSH]$_{ER}$ and speed of Kar2 oxidation are

proportionate to the amount of tunicamycin used (Figures 6F–6I). We thus surmise that activation of glutathione transport under ER stress is an amplification of the process occurring during non-stress conditions.

This model was established in the HGT1 cell model because of its unique ability to very rapidly accumulate glutathione to fairly high levels. However, the $[glutathione]_{ER}$ levels reached in HGT1 cells were much higher than those reached both on Tm exposure and upon hyperactive Ero1 overproduction. We suggest that the high $[glutathione]_{ER}$ levels reached in HGT1 cells are the consequence of the rapidity of their buildup, occurring prior to the regulation of glutathione transport via the UPR-dependent activation of Ero1 that induces the Kar2-dependent negative regulatory loop.

Glutathione as the Main ER Reducing Power

Efficiency of denatured protein refolding by PDI in vitro is a function not of disulfide formation but of disulfide isomerization, for which reduced glutathione has a crucial role (Lyles and Gilbert, 1991). While several studies suggest that glutathione provides the reducing power for ER oxidative folding and buffering Ero1 oxidizing activity (Chakravarthi and Bulleid, 2004; Cuozzo and Kaiser, 1999; Molteni et al., 2004), the observation that oxidative folding remains intact upon purging the mammalian ER of glutathione has suggested that it is dispensable in the ER (Tsunoda et al., 2014). However, the importance of glutathione-to-ER redox control is supported by the observation that glutathione becomes a potent ER reducing power when present at high levels (Kumar et al., 2011), and the current data indicate a net ER import of reduced glutathione, at least under Tm-induced ER stress, followed by Ero1 reductive activation. The 2-fold concerted increase in $[glutathione]_{Cyt}$ and $[glutathione]_{ER}$ and corresponding E_{GSH} decrease from −240 to −257 mV on Tm exposure, together with the consequential Ero1 activation, is a probable adaptive measure to ER stress protein misfolding. ER stress also stimulates glutathione biosynthesis in *A. thaliana* (Ozgur et al., 2015) and mammals by PERK-dependent Atf4 induction (Harding et al., 2003). Furthermore, ER stress caused by Tm in Atf4-deficient *C. elegans* (Harding et al., 2003) and by coagulation factor VIII expression in mouse hepatocytes (Malhotra et al., 2008) is associated with a 50% decrease in total glutathione levels. In *C. elegans*, this decrease is rescued by inactivating Ero1, which highlights the conservation of the functional interplay between glutathione and Ero1 established here, as well as the importance of glutathione for ER redox metabolism.

ER Transport of Glutathione by Idle Ribosome-Bound Translocons

Our data provide compelling evidence that both Sec61 and Ssh1 serve as glutathione conduits to the ER while ruling out a role of the Sec complex (Figures 3, 4, and S3). The presence of both gain and loss of function associated with Sec61 genetic modifications, and the absence of effect of the translation inhibitor puromycin, rule out an indirect effect. Inhibition of glutathione transport by oxidized Kar2, which contributes to the Sec61 polypeptide translocation mechanism (Mandon et al., 2013), further supports this conclusion. The aggravation of the $Sec61^{N302L}$ glutathione transport defect by deletion of *SSH1* (Figure 4D) indicates that both Sec61 and Ssh1 transport glutathione. The existence of another transporter cannot be ruled out, but it would have a minor function, given the major glutathione phenotypes of the *SEC61* mutants. Translocons are present in the ER membrane as unbound or bound by inactive or active ribosomes (Reid and Nicchitta, 2015). Those bound by active ribosomes do not allow glutathione transport, as indicated by total transport inhibition by CHX, which traps the nascent chain within the channel by blocking the translocation step in translation elongation (Schneider-Poetsch et al., 2010). Of the two remaining states of Sec61, the ones bound by idle ribosomes are those that appear permissive to glutathione transport, as suggested by partial transport inhibition upon $Srp54^{dn}$ overproduction (Figure 4J). By sequestering the SRP receptor into an inactive pool (Mutka and Walter, 2001), this mutant should decrease the ER content of both active and inactive ribosome-bound translocons, but the former are excluded by the effect of CHX. This conclusion is consistent with in vitro electrophysiological data that indicate that ER membrane permeability to ions and small molecules is due to idle ribosome-bound pores in both mammals and prokaryotes (Heritage and Wonderlin, 2001; Knyazev et al., 2013; Lizák et al., 2006; Simon and Blobel, 1991). It is also compatible with the structural changes of the channel triggered by idle ribosome binding, which consist of a partial opening of the lateral gate together with destabilization of the interaction between the plug and pore ring (Pfeffer et al., 2015; Zimmer et al., 2008). Disruption of plug-ring interactions might thus suffice to allow glutathione-facilitated diffusion.

Channel gating of glutathione by idle ribosomes raises the question of their availability. In semi-permeabilized mammalian cells, puromycin increases Sec61-dependent transport of a small molecule above a basal level, which indicates recruitment of additional pores (Heritage and Wonderlin, 2001). In contrast, the ER transport of glutathione is insensitive to puromycin, which suggests the presence of an invariant number of idle ribosome-bound translocons dedicated to glutathione transport.

Translocon Gating by Oxidized Kar2 Regulates the ER Transport of Glutathione

Mutation in the lateral gate motif ($Sec61^{N302L}$) (Trueman et al., 2012) and deletion of loop 7 ($Sec61\Delta L7$) (Tretter et al., 2013), which both stabilize the closed channel conformation, almost totally inhibited glutathione transport (Figures 4C and 4D). This observation could indicate that transport is allowed only when the channel is in the open conformation. However, the N302D mutation that stabilizes the open conformation (Trueman et al., 2012) did not impact transport (Figure 4E), whereas deletion of the plug domain (Δplug), which also stabilizes the channel open conformation (Junne et al., 2006; Trueman et al., 2012), resulted in the loss of glutathione transport inhibition (Figures 4F and 4G), as also seen with $Kar2^{C63A}$ and oxidized Kar2 (Figures 5G–5J). The latter data thus rather suggest that the plug is the critical Sec61 structural feature in glutathione gating. In mammals, binding of the Kar2 mammalian homolog Bip to loop 7 prevents Sec61-dependent ER leakage of calcium, presumably by inducing pore closure (Schäuble et al., 2012). From this result, we infer that oxidized Kar2 in yeast binds to loop 7, thereby reversing the idle ribosome-induced partial open

conformation and, in particular, restoring the plug-ring interactions (see above). The much higher values of $[GSx]_{ER}$ relative to $[GSx]_{Corr.Cyt}$ during the declining phase of the glutathione response indicated that facilitated diffusion governing the ER import of glutathione did not operate in reverse (Figure 2A). This result might be explained by either channel closure by oxidized Kar2 or direction of plug domain displacement within the pore lumenal face only allowing a cytosol-to-ER flux. However, the Sec61-dependent ER leakage of calcium upon Bip depletion (Schäuble et al., 2012) supports the former hypothesis.

Two distinct models have been proposed regarding regulation of the channel permeability barrier in the ER. In prokaryotes, the plug domain has been suggested to play a critical role (Park and Rapoport, 2012), while in eukaryotes, Bip/Kar2 fulfills this function (Hamman et al., 1998). Our data reconcile these two models by showing that the ER protein channel is in fact permeable, but this permeability is not constitutive but regulated in yeast by both oxidized Bip and the plug domain. From the ER transport of glutathione demonstrated here, we suggest that the ER membrane is permissive to the facilitated diffusion of any small molecule with a size at least equivalent to that of glutathione.

STAR★METHODS

Detailed methods are provided in the online version of this paper and include the following:

- KEY RESOURCES TABLE
- CONTACT FOR REAGENTS AND RESOURCE SHARING
- EXPERIMENTAL MODEL AND SUBJECT DETAILS
  - *S. cerevisiae*
- METHOD DETAILS
  - Reagents
  - Plasmids
  - RNA preparation, cDNA synthesis, and Quantitative RT-PCR analysis
  - Glutathione tolerance and survival assays
  - Redox westerns
  - Glutathione enzymatic measurement
  - Calculation of redox potentials and GSH/GSSG
  - Calculation of the absolute glutathione concentration
  - Live cell fluorescence microscopy
  - Subcellular fractionation
- QUANTIFICATION AND STATISTICAL ANALYSIS
  - Western blot quantification
  - Total cellular glutathione ($[GSx]_{TotCell}$) measurements
  - Survival assay

SUPPLEMENTAL INFORMATION

Supplemental Information includes six figures and two tables and can be found with this article online at http://dx.doi.org/10.1016/j.molcel.2017.08.012.

AUTHOR CONTRIBUTIONS

M.B.T., C.E.O., A.D.-M., B.D., and J.R.W. conceived and designed the experiments. M.B.T. wrote the manuscript. A.P., A.I., M.A.D., A.D.-M., G.P., and S.M. performed the experiments.

ACKNOWLEDGMENTS

We are indebted to C. Sevier, R. Gilmore, K. Romisch, P. Walter, and M. Spiess for their generous gifts of strains and plasmids. Thanks to R. Sitia for his comments on the manuscript. This work was funded by grants from the ANR (ERRed) and InCA (PLBIO INCA_5869) to M.B.T. and by NIH grants GM086619 and GM118164 to C.E.O. A.P. was supported by a CEA IRTELIS PhD fellowship.

Received: October 14, 2016
Revised: June 29, 2017
Accepted: August 18, 2017
Published: September 14, 2017

REFERENCES

Bánhegyi, G., Lusini, L., Puskás, F., Rossi, R., Fulceri, R., Braun, L., Mile, V., di Simplicio, P., Mandl, J., and Benedetti, A. (1999). Preferential transport of glutathione versus glutathione disulfide in rat liver microsomal vesicles. J. Biol. Chem. *274*, 12213–12216.

Björnberg, O., Ostergaard, H., and Winther, J.R. (2006). Measuring intracellular redox conditions using GFP-based sensors. Antioxid. Redox Signal. *8*, 354–361.

Brachmann, C.B., Davies, A., Cost, G.J., Caputo, E., Li, J., Hieter, P., and Boeke, J.D. (1998). Designer deletion strains derived from Saccharomyces cerevisiae S288C: a useful set of strains and plasmids for PCR-mediated gene disruption and other applications. Yeast *14*, 115–132.

Cary, G.A., Yoon, S.H., Torres, C.G., Wang, K., Hays, M., Ludlow, C., Goodlett, D.R., and Dudley, A.M. (2014). Identification and characterization of a drug-sensitive strain enables puromycin-based translational assays in Saccharomyces cerevisiae. Yeast *31*, 167–178.

Chakravarthi, S., and Bulleid, N.J. (2004). Glutathione is required to regulate the formation of native disulfide bonds within proteins entering the secretory pathway. J. Biol. Chem. *279*, 39872–39879.

Cuozzo, J.W., and Kaiser, C.A. (1999). Competition between glutathione and protein thiols for disulphide-bond formation. Nat. Cell Biol. *1*, 130–135.

Delaunay, A., Isnard, A.D., and Toledano, M.B. (2000). H2O2 sensing through oxidation of the Yap1 transcription factor. EMBO J. *19*, 5157–5166.

Delic, M., Mattanovich, D., and Gasser, B. (2010). Monitoring intracellular redox conditions in the endoplasmic reticulum of living yeasts. FEMS Microbiol. Lett. *306*, 61–66.

Desaint, S., Luriau, S., Aude, J.C., Rousselet, G., and Toledano, M.B. (2004). Mammalian antioxidant defenses are not inducible by H2O2. J. Biol. Chem. *279*, 31157–31163.

Deshaies, R.J., and Schekman, R. (1987). A yeast mutant defective at an early stage in import of secretory protein precursors into the endoplasmic reticulum. J. Cell Biol. *105*, 633–645.

Deshaies, R.J., and Schekman, R. (1990). Structural and functional dissection of Sec62p, a membrane-bound component of the yeast endoplasmic reticulum protein import machinery. Mol. Cell. Biol. *10*, 6024–6035.

Frand, A.R., and Kaiser, C.A. (1998). The ERO1 gene of yeast is required for oxidation of protein dithiols in the endoplasmic reticulum. Mol. Cell *1*, 161–170.

Frand, A.R., and Kaiser, C.A. (1999). Ero1p oxidizes protein disulfide isomerase in a pathway for disulfide bond formation in the endoplasmic reticulum. Mol. Cell *4*, 469–477.

Hamman, B.D., Hendershot, L.M., and Johnson, A.E. (1998). BiP maintains the permeability barrier of the ER membrane by sealing the lumenal end of the translocon pore before and early in translocation. Cell *92*, 747–758.

Harding, H.P., Zhang, Y., Zeng, H., Novoa, I., Lu, P.D., Calfon, M., Sadri, N., Yun, C., Popko, B., Paules, R., et al. (2003). An integrated stress response regulates amino acid metabolism and resistance to oxidative stress. Mol. Cell *11*, 619–633.

Heritage, D., and Wonderlin, W.F. (2001). Translocon pores in the endoplasmic reticulum are permeable to a neutral, polar molecule. J. Biol. Chem. *276*, 22655–22662.

Hu, J., Dong, L., and Outten, C.E. (2008). The redox environment in the mitochondrial intermembrane space is maintained separately from the cytosol and matrix. J. Biol. Chem. *283*, 29126–29134.

Iversen, R., Andersen, P.A., Jensen, K.S., Winther, J.R., and Sigurskjold, B.W. (2010). Thiol-disulfide exchange between glutaredoxin and glutathione. Biochemistry *49*, 810–820.

Junne, T., Schwede, T., Goder, V., and Spiess, M. (2006). The plug domain of yeast Sec61p is important for efficient protein translocation, but is not essential for cell viability. Mol. Biol. Cell *17*, 4063–4068.

Knyazev, D.G., Lents, A., Krause, E., Ollinger, N., Siligan, C., Papinski, D., Winter, L., Horner, A., and Pohl, P. (2013). The bacterial translocon SecYEG opens upon ribosome binding. J. Biol. Chem. *288*, 17941–17946.

Kumar, C., Igbaria, A., D'Autreaux, B., Planson, A.G., Junot, C., Godat, E., Bachhawat, A.K., Delaunay-Moisan, A., and Toledano, M.B. (2011). Glutathione revisited: a vital function in iron metabolism and ancillary role in thiol-redox control. EMBO J. *30*, 2044–2056.

Lizák, B., Czegle, I., Csala, M., Benedetti, A., Mandl, J., and Bánhegyi, G. (2006). Translocon pores in the endoplasmic reticulum are permeable to small anions. Am. J. Physiol. Cell Physiol. *291*, C511–C517.

Lyles, M.M., and Gilbert, H.F. (1991). Catalysis of the oxidative folding of ribonuclease A by protein disulfide isomerase: dependence of the rate on the composition of the redox buffer. Biochemistry *30*, 613–619.

Malhotra, J.D., Miao, H., Zhang, K., Wolfson, A., Pennathur, S., Pipe, S.W., and Kaufman, R.J. (2008). Antioxidants reduce endoplasmic reticulum stress and improve protein secretion. Proc. Natl. Acad. Sci. USA *105*, 18525–18530.

Mandon, E.C., Trueman, S.F., and Gilmore, R. (2013). Protein translocation across the rough endoplasmic reticulum. Cold Spring Harb. Perspect. Biol. *5*, a013342.

Margittai, E., and Sitia, R. (2011). Oxidative protein folding in the secretory pathway and redox signaling across compartments and cells. Traffic *12*, 1–8.

Massaad, M.J., and Herscovics, A. (2001). Interaction of the endoplasmic reticulum alpha 1,2-mannosidase Mns1p with Rer1p using the split-ubiquitin system. J. Cell Sci. *114*, 4629–4635.

Massaad, M.J., Franzusoff, A., and Herscovics, A. (1999). The processing alpha1,2-mannosidase of Saccharomyces cerevisiae depends on Rer1p for its localization in the endoplasmic reticulum. Eur. J. Cell Biol. *78*, 435–440.

Merksamer, P.I., Trusina, A., and Papa, F.R. (2008). Real-time redox measurements during endoplasmic reticulum stress reveal interlinked protein folding functions. Cell *135*, 933–947.

Molteni, S.N., Fassio, A., Ciriolo, M.R., Filomeni, G., Pasqualetto, E., Fagioli, C., and Sitia, R. (2004). Glutathione limits Ero1-dependent oxidation in the endoplasmic reticulum. J. Biol. Chem. *279*, 32667–32673.

Montero, D., Tachibana, C., Rahr Winther, J., and Appenzeller-Herzog, C. (2013). Intracellular glutathione pools are heterogeneously concentrated. Redox Biol. *1*, 508–513.

Morgan, B., Ezeriņa, D., Amoako, T.N., Riemer, J., Seedorf, M., and Dick, T.P. (2013). Multiple glutathione disulfide removal pathways mediate cytosolic redox homeostasis. Nat. Chem. Biol. *9*, 119–125.

Mutka, S.C., and Walter, P. (2001). Multifaceted physiological response allows yeast to adapt to the loss of the signal recognition particle-dependent protein-targeting pathway. Mol. Biol. Cell *12*, 577–588.

Østergaard, H., Tachibana, C., and Winther, J.R. (2004). Monitoring disulfide bond formation in the eukaryotic cytosol. J. Cell Biol. *166*, 337–345.

Ozgur, R., Uzilday, B., Sekmen, A.H., and Turkan, I. (2015). The effects of induced production of reactive oxygen species in organelles on endoplasmic reticulum stress and on the unfolded protein response in arabidopsis. Ann. Bot. (Lond.) *116*, 541–553.

Park, E., and Rapoport, T.A. (2012). Mechanisms of Sec61/SecY-mediated protein translocation across membranes. Annu. Rev. Biophys. *41*, 21–40.

Pfeffer, S., Burbaum, L., Unverdorben, P., Pech, M., Chen, Y., Zimmermann, R., Beckmann, R., and Förster, F. (2015). Structure of the native Sec61 protein-conducting channel. Nat. Commun. *6*, 8403.

Pollard, M.G., Travers, K.J., and Weissman, J.S. (1998). Ero1p: a novel and ubiquitous protein with an essential role in oxidative protein folding in the endoplasmic reticulum. Mol. Cell *1*, 171–182.

Reid, D.W., and Nicchitta, C.V. (2015). Diversity and selectivity in mRNA translation on the endoplasmic reticulum. Nat. Rev. Mol. Cell Biol. *16*, 221–231.

Rothblatt, J.A., Deshaies, R.J., Sanders, S.L., Daum, G., and Schekman, R. (1989). Multiple genes are required for proper insertion of secretory proteins into the endoplasmic reticulum in yeast. J. Cell Biol. *109*, 2641–2652.

Schäuble, N., Lang, S., Jung, M., Cappel, S., Schorr, S., Ulucan, Ö., Linxweiler, J., Dudek, J., Blum, R., Helms, V., et al. (2012). BiP-mediated closing of the Sec61 channel limits Ca2+ leakage from the ER. EMBO J. *31*, 3282–3296.

Schneider-Poetsch, T., Ju, J., Eyler, D.E., Dang, Y., Bhat, S., Merrick, W.C., Green, R., Shen, B., and Liu, J.O. (2010). Inhibition of eukaryotic translation elongation by cycloheximide and lactimidomycin. Nat. Chem. Biol. *6*, 209–217.

Sevier, C.S., Qu, H., Heldman, N., Gross, E., Fass, D., and Kaiser, C.A. (2007). Modulation of cellular disulfide-bond formation and the ER redox environment by feedback regulation of Ero1. Cell *129*, 333–344.

Simon, S.M., and Blobel, G. (1991). A protein-conducting channel in the endoplasmic reticulum. Cell *65*, 371–380.

Toledano, M.B., Kumar, C., Le Moan, N., Spector, D., and Tacnet, F. (2007). The system biology of thiol redox system in Escherichia coli and yeast: differential functions in oxidative stress, iron metabolism and DNA synthesis. FEBS Lett. *581*, 3598–3607.

Tretter, T., Pereira, F.P., Ulucan, O., Helms, V., Allan, S., Kalies, K.U., and Römisch, K. (2013). ERAD and protein import defects in a sec61 mutant lacking ER-lumenal loop 7. BMC Cell Biol. *14*, 56.

Trueman, S.F., Mandon, E.C., and Gilmore, R. (2012). A gating motif in the translocation channel sets the hydrophobicity threshold for signal sequence function. J. Cell Biol. *199*, 907–918.

Tsunoda, S., Avezov, E., Zyryanova, A., Konno, T., Mendes-Silva, L., Pinho Melo, E., Harding, H.P., and Ron, D. (2014). Intact protein folding in the glutathione-depleted endoplasmic reticulum implicates alternative protein thiol reductants. eLife *3*, e03421.

Tu, B.P., and Weissman, J.S. (2002). The FAD- and O(2)-dependent reaction cycle of Ero1-mediated oxidative protein folding in the endoplasmic reticulum. Mol. Cell *10*, 983–994.

Wang, J., Pareja, K.A., Kaiser, C.A., and Sevier, C.S. (2014). Redox signaling via the molecular chaperone BiP protects cells against endoplasmic reticulum-derived oxidative stress. eLife *3*, e03496.

Zimmer, J., Nam, Y., and Rapoport, T.A. (2008). Structure of a complex of the ATPase SecA and the protein-translocation channel. Nature *455*, 936–943.

STAR★METHODS

KEY RESOURCES TABLE

REAGENT or RESOURCE	SOURCE	IDENTIFIER
Antibodies		
anti-Myc monoclonal	A gift from C. Créminon, Saclay, France	9E10
Rabbit polyclonal anti-GFP	Life Technologies	A-6455; RRID: AB_221570
Anti-Kar2 polyclonal (y115)	Santa Cruz	SC-33630; RRID: AB_672118
Chemicals, Peptides, and Recombinant Proteins		
Glutathione	Sigma-Aldrich	G 4251
Diamide	Sigma-Aldrich	D3648-5G
Dithiothreitol (DTT)	Sigma-Aldrich	D0632
Puromycin	Sigma-Aldrich	P8833-100MG
Cycloheximide	Sigma-Aldrich	C 4859
Methoxypolyethylene glycol maleimide (PEG-maleimide) 2,000	Sigma-Aldrich	731765
Methoxypolyethylene glycol maleimide (PEG-maleimide) 5,000	Sigma-Aldrich	63187-1G
N-ethylmaleimide (NEM)	Sigma-Aldrich	E 3876-5G
5,5′-dithiobis (2 nitrobenzoic acid) (DTNB)	Sigma-Aldrich	D8130-1G
Critical Commercial Assays		
NucleoSpin RNA plus	Macherey Nagel	740984.250
M-MLV RT	Invitrogen	28025013
micro BCA kit	Pierce	23235
NuPAGE Novex 4-12% Bis-Tris Protein Gels, 1.5 mm, 15-well	Ugap	NP0336BOX
Experimental Models: Organisms/Strains		
MATα his3Δ1, leu2Δ0, lys2Δ0, ura3Δ0	Brachmann et al., 1998	BY4742
BY4742 *ire1::kanMX4*	Brachmann et al., 1998	BY4742 Δ*ire1*
BY4742 *hac1::kanMX4*	Brachmann et al., 1998	BY4742 Δ*hac1*
BY4742 *gsh1::kanMX4*	Brachmann et al., 1998	BY4742 Δ*gsh1*
MATa GAL2 ura3-52 leu2-3,112	Frand and Kaiser, 1998	CKY263
MATa GAL2 ero1-1 ura3-52 leu2-3,112	Frand and Kaiser, 1998	CKY598
MATα sec61-2 pep4-3 ade2-1 ura3-52 leu2-3,-112	Deshaies and Schekman, 1987	RSY524
MATα ura3-52 leu2-3,112 pep4-3 s63-1	Rothblatt et al., 1989	RSY151
MATα his4 leu2-3,112 ura3-52 s62-1	Deshaies and Schekman, 1990	RSY529
MATa ura3-1 leu2-3,112 his3-11,15 trp1-1 ade2-1 can1-100 s61::HIS3 [pDQ1])	Junne et al., 2006)	RSY1293
MATα trp1-1 ade2 leu2-3,112 ura3 his3-11 can1 s61::HIS3 [pEM299]	Trueman et al., 2012	EMY101
MATα trp1-1 ade2 leu2-3,112 ura3 his3-11 ssh1::kanMX4 s61::HIS3 [pEM299]	Trueman et al., 2012	EMY102
Δ*egr6* Δ*pdr1* Δ*pdr3*	Cary et al., 2014	YAD337
MATa GAL2 ura3-52 leu2-3,112	Wang et al., 2014	CKY263/CSY5
MATa GAL2 ura3-52 leu2-3,112 kar2-C63A	Wang et al., 2014	CSY275

(*Continued on next page*)

Continued

REAGENT or RESOURCE	SOURCE	IDENTIFIER
Oligonucleotides		
KAR2 forward primer 5′-TGATAACTTTGAAACCATTG-3′	Sigma-Aldrich	None
KAR2 reverse primer 5′-TAATTGGATAAGCGACCTTGGA-3′	Sigma-Aldrich	None
ACT1 forward primer 5′-TGTCACCAACTGGGACGATA-3′	Sigma-Aldrich	None
ACT1 REVERSE PRIMER 5′-AACCAGCGTAAATTGGAACG-3′	Sigma-Aldrich	None
Recombinant DNA		
CEN LEU2 ER-rxYFP	This study	pRS315 ER-rxYFP
CEN LEU2 Cyt-rxYFP	This study	pRS315 Cyt-rxYFP
CEN URA3 p*TEF-HGT1*	Kumar et al., 2011	pRS416 pTEF*HGT1*
Integrative *LEU2* ERrxYFP-grx1 derived from pJW2011	This study	pRS304 ER-rxYFP-Grx1
CEN LEU2 p*TEF*-ER grx1-1cys	This study	pTEF415 ER-1-Cys-Grx1
CEN LEU2 p*TEF*-cyt grx1-1cys	This study	pTEF415 Cyt-1-Cys-Grx1
CEN URA3 p*GAL1-ERO1-MYC*	Sevier et al., 2007	pAF112
CEN URA3 p*GAL1-ERO1*-MYC*	Sevier et al., 2007	pCS452
CEN LEU2 MYC-ERO1	Sevier et al., 2007	pAF85
pGAL-*SRP54*^{DN} (*TRP1, CEN6/ARSH4*)	Mutka and Walter, 2001	pSM110
pGAL-*SRP54* (*TRP1, CEN6/ARSH4*)	Mutka and Walter, 2001	pSM131
(2μ, *LEU2*) *SEC61*	This study	pSec61
(*LEU2 CEN*) *SEC61*	Junne et al., 2006	pDQ1
(*LEU2 CEN*) *sec61*Δplug	Junne et al., 2006	pYC-plac111
pRS316 *URA3 SEC61-V5 (URA3, CEN)*	Trueman et al., 2012	pEM299
pRS315 *sec61 N302D*	Trueman et al., 2012	pEM635
pRS315 *sec61 N302L*	Trueman et al., 2012	pEM634
pRS315 *SEC61*	Tretter et al., 2013	pRS315 Sec61
pRS315 *sec61ΔL7*	Tretter et al., 2013	pRS315 *sec61ΔL7*
pRS315 *KAR2 CEN LEU2*	Wang et al., 2014	pCS681
pRS315 *KAR2-C63W CEN LEU2*	Wang et al., 2014	pCS750
Software and Algorithms		
ImageJ (western blot image quantifications)	https://imagej.nih.gov/ij/	None
GraphPad prism 6 (Figures creation)	GraphPad	None
QuantPrime software	http://quantprime.mpimp-golm.mpg.de/	None

CONTACT FOR REAGENTS AND RESOURCE SHARING

Further information and requests for resources and reagents should be directed to and will be fulfilled by the Lead Contact, Michel B. Toledano (Michel.toledano@cea.fr)

EXPERIMENTAL MODEL AND SUBJECT DETAILS

S. cerevisiae

Strains used in this study and information regarding their genotype can be found in the Key Resources Table and in Table S1. Strains are derivative of BY4741, BY4742 or, as indicated in Table S1. Cells were cultured at 30°C, or as indicated, in YPD (1% yeast extract, 2% peptone and 2% glucose), minimal media (SD) (0.67% yeast nitrogen base w/o amino acids, 2% glucose), or galactose medium with amino acid supplements, as indicated.

METHOD DETAILS

Reagents

Chemicals

Glutathione, diamide, dithiothreithol, puromycin, cycloheximide, 5,5′-dithiobis (2 nitrobenzoic acid) (DTNB), N-ethylmaleimide (NEM) and methoxypolyethylene glycol maleimide (PEG-maleimide) 2,000 and 5,000 were purchased from SIGMA.

Antibodies

The 9E10 anti-Myc monoclonal antibody is a gift from C. Créminon, Saclay, France. rxYFP was revealed with rabbit polyclonal anti-GFP (Life Technologies), and Kar2 with a Kar2-specific antibody (Santa Cruz).

Plasmids

All plasmids used in this study can be found in the Key Resources Table and are listed in Table S2. pRS304-ER-rxYFP-Grx1 was constructed by PCR-based fusion of the Mns1 ER targeting sequence at the 5′ end (Massaad et al., 1999; Massaad and Herscovics, 2001) and the HDEL retention signal sequence at the 3′ end of cytosolic rxYFP-Grx1 (Björnberg et al., 2006). The Mns1-rxYFP-Grx1-HDEL DNA fusion was then integrated between the *Mlu*I and *Spe*I sites of pRS304, downstream to the *PGK1* promoter, thus replacing the entire ER-rxYFP sequence in pHOJ150 (Østergaard et al., 2004). pRS315-ER-rxYFP was constructed by subcloning the coding sequence of ER-rxYFP from pHOJ150 (Østergaard et al., 2004) between the *Not*I and *Sac*II sites of pRS315. pRS315-Cyt-rxYFP was similarly constructed by subcloning the Cyt-rxYFP coding sequence from pJH208 (Hu et al., 2008) into pRS315. The ER-1-Cys-Grx1 probe was synthesized (Eurofins MWG Operon) by fusion from the 5′ end the *MNS1* signal sequence, three copies of the Myc tag sequence, the yeast *GRX1* sequence carrying a Cys30 to Ser substitution, and the HDEL ER retrieving signal sequence. The fusion gene was cloned between the BamHI and *Hind*III sites of pTEF415, downstream of the TEF promoter. The Cyt-1-Cys-Grx1 probe was similarly constructed without the *MNS1* and *HDEL* sequences. The eroGFP probe (Merksamer et al., 2008), was modified by insertion of a 15-amino acid glycosylation site before the HDEL.

RNA preparation, cDNA synthesis, and Quantitative RT-PCR analysis

mRNA was extracted using NucleoSpin RNA (Macherey Nagel). Quantitative RT-PCR used unique oligonucleotide primer pairs designed by the QuantPrime software and assayed for efficiency > 90% and specificity. Total RNA (6 μg) was M-MLV-reversed transcribed using random hexanucleotides as primers, and quantitative PCR was performed in triplicate as described (Desaint et al., 2004).

Glutathione tolerance and survival assays

For plate assays, tolerance to HGT1-dependent GSH toxicity was assessed by spotting 5 μL on plates containing various amounts of GSH via serial dilution of cell cultures in exponential growth phase.

For the GSH survival assays, cultures of exponential-phase cells were divided in two, one receiving GSH at various concentrations and the other no added GSH. At the indicated times, cells were collected, counted using a coulter counter, and spread on YPD plates at a density of approximately 200 CFU/plate. Three independent biological replicates and at least two technical replicates were performed. Plates were incubated 3 days at 30°C and CFU were counted. The percentage of survival was calculated using the untreated culture as 100%.

Redox westerns

Samples were collected from cell growing in exponential phase by the addition in the culture medium of pure TCA to a final concentration of 20% and immediately stored on ice. After centrifugation, the cells were washed with 20% TCA and frozen at −80°C. Protein extraction and alkylation were performed as previously described (Delaunay et al., 2000). For rxYFP, after cell disruption by the glass beads shaking method in the presence of trichloroacetic acid (TCA) (20% final), precipitated proteins were dissolved in SB buffer (100 mM Tris–Cl pH 8, 1% SDS) containing 50 mM N-ethylmaleimide (NEM) and incubated 1 hr at RT in the dark. Protein concentration was measured by bicinchoninic acid-based colorimetric detection (micro BCA kit, Pierce), and the protein sample was separated by non-reducing SDS-polyacrylamide gel electrophoresis (4%–12% NuPAGE precasted gels, Life technologies, USA). For 1-Cys-Grx1 and Kar2, following protein-TCA precipitation, free reduced Cys residues were alkylated in the presence of 50 mM NEM for 1 hr at RT in the dark, then proteins were again precipitated with TCA, and the precipitated pellet washed 3 times with cold acetone. Samples were then dissolved in sample SB buffer, incubated 15 min with 200 mM DTT and again TCA precipitated. After three washes the protein pellet was resuspended in SB buffer containing 30 mM PEG-maleimide 5,000 (Kar2) or 2,000 (1-Cys-Grx1) for 20 min at RT in the dark. Samples were then separated by reducing SDS-PAGE (SDS-PAGE 15% acrylamide (30;0,4 bis/acrylamide) for optimal 1-Cys-Grx1 separation and SDS-PAGE 10% acrylamide (30;0,4 bis/acrylamide) for Kar2). After gel electrophoresis and gel transfer, 1-Cys-Grx1 was revealed with the 9E10 anti-Myc monoclonal antibody (a gift from C. Créminon, Saclay, France), rxYFP with rabbit polyclonal anti-GFP (Life Technologies), and a Kar2-specific antibody (Santa Cruz). Primary antibodies were then revealed with anti-mouse IgG or anti-rabbit IgG secondary antibodies labeled with fluorophores of different wavelengths, followed by Infrared Imaging technology (Odyssey, LI-COR). The reduced-to-oxidized ratio of rxYFP and 1-Cys-Grx1 was quantified using the ImageJ software.

Glutathione enzymatic measurement

Total and oxidized glutathione were measured using the Ellman's reagent, 5,5′-dithiobis (2 nitrobenzoic acid) (DTNB, SIGMA) colorimetric assay. Ten units (OD_{600}) of a cell suspension was washed in water, pelleted, and frozen at −80°C in 1% sulfosalicylic acid (SSA). Upon thawing, cells were disrupted by the glass beads shaking method, and kept on ice for 30 min, followed by centrifugation at 16000 rpm for 15 min at 4°C, and the supernatant was recovered. For total glutathione determination, 5-20 μl of the cell supernatant was added to the reaction buffer (0.1 M sodium phosphate, pH 7.5, 1 mM EDTA, 0.2 mM NADPH, and 0.2 mM DTNB) pre-warmed at 30°C; the reaction was initiated by addition of 1 Unit glutathione reductase (SIGMA), and the change of absorbance at 412 nm was measured using a spectrophotometer for 1 min. For GSSG determination, 2 μl of 2-vinylpyridine and 2 μl of 25% triethanolamine were added to 100 μl of the cell supernatant, in order to raise the pH and alkylate GSH. Samples were kept 1 hr at room temperature, then 5-20 μl were used in the DTNB recycling assay.

The cellular concentrations of total glutathione ($[GSx]_{TotCell}$) and GSSG ($[GSSG]_{TotCell}$) were determined based on a GSx and GSSG standard titration curves, and on the basis of an estimated average cell volume of 48 μm^3 and the cell number of the particular sample determined by the number of colony-forming units upon plating serial dilutions of the cell suspension on YPD-agar plates. Accordingly, measurements took into account cellular loss during experiments.

Calculation of redox potentials and GSH/GSSG

The reduced-to-oxidized rxYFP ratio was used to calculate E_{GSH} using the Nernst equation:

$$E_{GSH} = E^{o'}_{GSH} - (60.1\ \text{mV}/2)\ \log[GSH]^2 \Big/ [GSSG] = E^{o'}_{rxYFP} - (60.1\ \text{mV}/2)\ \log(rxYFP_{red})/(rxYFP_{ox}) = E_{rxYFP}. \quad \text{(Equation 1)}$$

With $E^{o'}{}_{GSH} = -240$ mV and $E^{o'}{}_{rxYFP} = -265$ mV, at pH 7.

The reduced-to-oxidized 1-Cys-Grx1 ratio was used to calculate R_{GS} = [GSH]/[GSSG], as described (Montero et al., 2013), according to Equation 2:

$$\text{1-Cys-Grx1pSH} + \text{GSSG} \rightleftarrows \text{1-Cys-Grx1pSSG} + \text{GSH} \quad \text{(Equation 2)}$$

and to a K_{ox} of 74 ± 6 (Iversen et al., 2010)

$$R_{GS} = \frac{[GSH]}{[GSSG]} = K_{ox}\frac{[1 - Cys - Grx1pSH]}{[1 - Cys - Grx1pSSG]}.$$

Calculation of the absolute glutathione concentration

To calculate the absolute glutathione concentration [GSx], we used $[GSH]^2/[GSSG]$ derived from the E_{GSH} values, and the values of R_{GS} as described (Montero et al., 2013):

$$[GS_X] = \left\{ \left([GSH]^2 \Big/ [GSSG] \right) \Big/ R_{GS} \right) + 2 \right\} \times \left\{ \left([GSH]^2 \Big/ [GSSG] \right) \Big/ R^2_{GS} \right).$$

Live cell fluorescence microscopy

Exponential phase grown cells were imaged using a Leica TCS SP2 confocal scanning microscope with an excitation wavelength for GFP at 488 nm and selection of emitted light of 500–570 nm.

Subcellular fractionation

Spheroplasts obtained by treatment of a cell suspension with Zymolyase were disrupted by osmotic shock. After discarding non-disrupted cells by low speed centrifugation (2000 g), the supernatent was fractionated by centrifugation at 13,000 *g* between pellet, containing membranes (P), and supernatant, containing the cytosol (S).

QUANTIFICATION AND STATISTICAL ANALYSIS

All data of the manuscript are presented as the average ± Standard Deviation (±SD). All experiments were performed at least four times. The values of $[GSx]_{TotCell}$, $[GSx]_{Corr\text{-}TotCell}$, $[GSx]_{Cyt}$, $[GSx]_{ER}$, $[GSH/GSSG]_{ER}$, $E_{GSH.Cyt}$, $E_{GSH.ER}$ shown in all the figures of the manuscript represent the average from three independent biological replicate, and the SD is represented as error bars. No methods were used to determine whether the data met assumptions of the statistical approach.

Western blot quantification

Western blots were performed as described in the Method Details. Raw images where quantified using the ImageJ software. Band areas were boxed and backgrounds were subtracted. Figures 1D and 2D display representative western blots performed with the ER-rxYFP and ER-1-Cys-Grx1, respectively.

Total cellular glutathione ($[GSx]_{TotCell}$) measurements

Glutathione measurements were performed as described in Method Details from three independent biological replicates.

Survival assay

Survival assays were performed as described in Method Details. Survival rates values are the average of three independent biological replicates and 3 to 5 technical repeats.